RSC Advances

PAPER

View Article Online
View Journal | View Issue

Cite this: *RSC Adv.*, 2025, **15**, 31060

Fabrication and characterization of electrospun polycaprolactone/*Urechis unicinctus* derived-ECM composite scaffolds for small-diameter vascular grafts

Jongwon Mun, Seung Pil Pack and Hyeongjin Lee *

Small-diameter vascular grafts (SDVGs; ≤6 mm inner diameter) often fail due to thrombosis, poor endothelialization, and low patency. To overcome these limitations, we developed electrospun composite scaffolds incorporating decellularized *Urechis unicinctus* ECM (UdECM), a marine invertebrate source rich in collagen, glycosaminoglycans, and elastin. UdECM was blended with polycaprolactone (PCL) at 1, 5, and 10 wt% and electrospun into fibrous matrices. We characterized scaffold hydrophilicity (water contact angle, water uptake), mechanical properties, and cell behaviors (*e.g.*, viability, proliferation, tube formation) using EA.hy926 endothelial cells, and performed *in vitro* blood clotting assays. UdECM-containing scaffolds exhibited improved hydrophilicity and mechanical strength compared to pure PCL, with the 10 wt% UdECM scaffold demonstrating the highest stiffness while retaining suitable elongation. Endothelial cells grown on UdECM-enhanced scaffolds showed increased viability and tube formation, indicative of a pro-angiogenic environment. Anticoagulant tests revealed reduced blood cell adhesion with higher UdECM content. These findings underscore the potential of marine-derived ECM to enhance the functionality of synthetic vascular grafts by promoting both endothelialization and thromboresistance.

Received 20th June 2025
Accepted 22nd August 2025

DOI: 10.1039/d5ra04406e

rsc.li/rsc-advances

Introduction

Cardiovascular diseases (CVDs) remain the leading cause of mortality worldwide, creating a critical demand for vascular grafts in bypass surgeries.[1,2] In particular, there is an acute need for small-diameter vascular grafts (SDVGs) for procedures such as coronary artery bypass and peripheral artery repair.[1–3] Autologous vessels (e.g., saphenous vein or internal mammary artery) are the gold-standard conduits due to their excellent biocompatibility and long-term patency.[3–6] However, autograft availability is limited a significant fraction of patients lack suitable autologous vessels because of prior harvest or disease,[4,5] and harvesting procedures can cause donor site morbidity.[7] Synthetic grafts made of materials like expanded polytetrafluoroethylene (ePTFE) or Dacron have been successful in large-diameter applications, but they consistently fail in small diameters due to acute thrombosis, low patency, and intimal hyperplasia caused by the hemodynamic conditions in narrower vessels.[8] Consequently, there is a compelling clinical impetus to develop a small-diameter vascular graft with patency and performance approaching native vessels.[9,10]

Tissue engineering offers a promising strategy to address this need by creating small-diameter vascular grafts (SDVGs) that combine biocompatible materials and cells to regenerate a functional blood vessel.[10] An ideal tissue-engineered vascular graft (TEVG) scaffold should be biocompatible, support endothelialization, possess appropriate mechanical strength and compliance, and degrade at a rate that promotes tissue remodeling without premature loss of integrity.[11] Electrospinning has emerged as a versatile technique to fabricate such scaffolds, as it produces nanofibrous membranes that closely mimic the architecture of native extracellular matrix (ECM).[12,13] Electrospun tubular scaffolds can be readily formed with controlled fiber diameter and porosity, facilitating cell attachment and infiltration while maintaining sufficient burst strength for implantation.[14,15] Indeed, many recent studies have adopted electrospun fibrous scaffolds for vascular graft applications, demonstrating favorable properties for guiding tissue regeneration and cell integration.[1,16,17]

Among candidate scaffold materials, poly(ε-caprolactone) (PCL) has been extensively used for vascular tissue engineering due to its FDA-approved biocompatibility, favorable biomechanical properties, and amenability to electrospinning.[18] PCL is a slowly biodegradable aliphatic polyester (degradation on the order of 2–3 years *in vivo*), which helps a graft maintain mechanical support during the critical initial months of vascular remodeling.[11] Electrospun PCL scaffolds have shown adequate tensile strength and suture retention for small vessel applications.[19,20] However, a well-known limitation of PCL is its

Department of Biotechnology and Bioinformatics, Korea University, Sejong 30019, Republic of Korea. E-mail: hyeongjinlee@korea.ac.kr; Tel: +82-44-860-1414

hydrophobic, bioinert surface that lacks cell-recognition motifs, often resulting in suboptimal endothelial cell adhesion and delayed endothelialization when used alone. Without modification, a pure PCL graft may risk thrombosis or intimal hyperplasia due to poor endothelial coverage.[20] Therefore, various strategies have been explored to improve the bioactivity of PCL-based vascular scaffolds, including surface functionalization, co-culture with cells, and blending with natural polymers or ECM components.[1,21]

Incorporating extracellular matrix (ECM) components into synthetic scaffolds is an effective approach to enhance their biocompatibility and biofunctional performance. Natural polymers such as collagen, elastin, gelatin, and fibrin inherently provide cell-attachment sites (*e.g.*, RGD sequences) and biochemical cues that promote cell adhesion, migration, and differentiation.[20–24] Blending or coating PCL scaffolds with collagen and gelatin for example, has been shown to significantly improve endothelial cell attachment and proliferation *in vitro* compared to pure PCL scaffolds.[20,23] Beyond single proteins, using whole decellularized ECM from tissues can offer a complex composition of collagen, glycosaminoglycans (GAGs), and growth factors, more closely resembling native microenvironments.[25] Decellularized natural scaffolds (such as acellular vascular graft, small intestinal submucosa) have demonstrated excellent biocompatibility and regenerative capacity by leveraging the retained ECM architecture and bioactive factors.[26] Nonetheless, decellularized tissue grafts from human or mammalian sources can be limited by donor tissue availability and potential immunogenicity if any residual antigens remain.[27] As a result, there is growing interest in alternative biomaterial sources, including those from marine organisms, to supply bioactive ECM components for tissue-engineered constructs. Marine invertebrates and fish are abundant and offer collagens and polysaccharides with low risk of transmitting human pathogens or triggering immune reactions, making them attractive for biomaterials research.[27–29] Nevertheless, prior PCL/ECM systems including PCL blended or coated with collagen or gelatin have only shown improvements in wettability and endothelialization over pure PCL.[20,23] Yet their reliance on single proteins seldom reconstructs an elastin- and sulfated-GAG-rich environment needed for compliance and hemocompatibility, motivating exploration of marine, multi-component dECM sources.[25–29] Although marine-derived dECM (and fish collagen/PCL hybrids) offer favorable biocompatibility and practical supply advantages,[30] evidence specific to small-diameter vascular graft applications remains limited.

Urechis unicinctus, commonly known as the spoon worm or sea intestine, has recently gained attention as a novel biomaterial source.[31–33] This *U. unicinctus* body wall is rich in type I collagen, constituting over 70% of its dry weight, as well as glycosaminoglycans (GAGs) that contribute to its connective tissue architecture.[34,35] These components underscore the *U. unicinctus* potential as a biomimetic structural matrix. In addition, *U. unicinctus* extracts exhibit promising bioactivities: GAGs show potent antiplatelet and anticoagulant effects, evidenced by *ex vivo* platelet assays and *in vitro* clotting tests suggesting antithrombogenic advantages for vascular grafts. Furthermore, neuronal peptides (*urechistachykinins* I and II) have antimicrobial activity without hemolysis, broadening this marine invertebrate's biomedical potential.[33,35,36] While *U. unicinctus* is commercially harvested along the Korean west coast, its biomedical use remains at an exploratory stage.

In this study, we utilized material obtained from existing harvesting streams to demonstrate its feasibility as a novel ECM source, without implying established clinical or large-scale biomedical application. Building on this premise, we therefore hypothesized that incorporating decellularized *U. unicinctus* ECM (UdECM) into an electrospun PCL scaffold would combine the robust mechanical properties of PCL with the bioactive, antithrombotic cues of the marine ECM, thereby enhancing the scaffold's performance as a SDVGs. To investigate this, we fabricated and characterized an electrospun PCL/UdECM composite scaffold, evaluated the scaffold micro-structure, hydrophilicity, mechanical properties, and cytocompatibility, and assessed its ability to support endothelial cell growth and *in vitro* blood clotting assays. Ultimately, by leveraging bioactive marine-derived ECM within a synthetic fiber matrix, our aim was to develop a hybrid scaffold that addresses the critical requirements of SDVGs namely biocompatibility, mechanical suitability, and resistance to thrombosis.

Materials and methods

Materials

Specimens of *Urechis unicinctus* (commonly known as the fat innkeeper worm) were harvested from the west coast of the Republic of Korea and obtained from a commercial supplier. Sodium dodecyl sulfate (SDS) and Triton™ X-100 (both from Sigma-Aldrich, USA) were used for decellularization. Poly(ε-caprolactone) (PCL; M_n = 80 000, Sigma-Aldrich, USA) was selected as the electrospinning polymer. For electrospinning solvents, 1,1,1,3,3,3-hexafluoro-2-propanol (HFIP; Daejeong Chemical, Korea) was employed. To achieve crosslinking, *N*-(3-dimethylaminopropyl)-*N*′-ethylcarbodiimide hydrochloride (EDC; Sigma-Aldrich, USA) and *N*-hydroxysuccinimide (NHS; Sigma-Aldrich, USA) were utilized. Pluronic® F-127 (Sigma-Aldrich, USA) was used to gently remove the crosslinked scaffolds from the stainless-steel mandrel.

Preparation of decellularized ECM from *Urechis unicinctus* (UdECM)

Prior to decellularization, both ends of *U. unicinctus* were trimmed to remove ciliated tissues. The body was longitudinally incised to extract internal organs and bodily fluids, followed by extensive washing with phosphate-buffered saline (PBS) to eliminate mucus. Cleaned body-wall tissues were cut into uniform sections (10 mm × 10 mm) and immersed in 1% SDS at 4 °C under gentle stirring for 3 days. Following this treatment, the decellularized tissues were washed three times with PBS, then incubated in 0.25% Triton™ X-100 at 4 °C for 24 h, and once again washed with PBS (three cycles) to remove any residual reagents. The resulting decellularized tissues were freeze-dried for 48 h and stored at −80 °C. For further

processing, the freeze-dried samples were cryo-milled (Freezer/Mill, Spex SamplePrep, NJ, USA) into fine powders, hereafter referred to as UdECM (Fig. S1). The UdECM powder was sealed and stored at −80 °C until use.

Quantification of DNA and ECM components in UdECM

To evaluate the degree of decellularization and the main ECM constituents in UdECM, DNA, collagen, sulfated glycosaminoglycans (sGAGs), and elastin were quantified using specialized assays. DNA was extracted using a Qiagen DNeasy Blood & Tissue Kit (Qiagen Inc., USA), and total DNA content was measured with a Quant-iT PicoGreen dsDNA Assay kit (Thermo Fisher Scientific, USA) according to the manufacturer's protocol. For collagen content, 20 mg of UdECM were digested in 0.5 M acetic acid containing 0.1% (w/v) pepsin at 4 °C for 24 h, followed by centrifugation at 3000×*g* for 10 min; the soluble fraction was analyzed with the Sircol™-2.0 Soluble Collagen Assay (Biocolor, UK). Sulfated glycosaminoglycans (sGAGs) were quantified using the Blycan™ Sulfated GAG Assay (Biocolor, UK) by incubating 20 mg of UdECM in papain extraction reagent at 65 °C for 3 h, then centrifuging at 10 000×*g* for 10 min to collect the supernatant. Elastin content was measured using the Fastin™ Elastin Assay Kit (Biocolor, UK), wherein 20 mg of UdECM were extracted in 0.25 M oxalic acid at 100 °C for 1 h, followed by centrifugation at 13 000×*g* for 10 min. Absorbance values for collagen, sGAGs, and elastin were recorded at 556 nm, 656 nm, and 513 nm, respectively, using a microplate reader (TECAN, Switzerland). All measurements were performed in triplicate, and data are expressed as mean ± standard deviation.

SDS–PAGE protein profiling

Protein composition in UdECM was further characterized by sodium dodecyl sulfate–polyacrylamide gel electrophoresis (SDS–PAGE). Freeze-dried UdECM (10 mg) was dissolved in 0.5 M acetic acid. After complete dissolution, 5× SDS sample loading buffer was added, and the mixture was incubated at 100 °C for 10 min to denature proteins. The denatured samples were loaded onto a 10% separating gel (4% stacking gel). Electrophoresis was initially run at 50 V for 10 min, followed by 110 V until sufficient protein separation was achieved.

Preparation of PCL/UdECM composite electrospinning solutions

Electrospinning solutions were prepared according to the compositions summarized in Table 1. UdECM powder was first dispersed in 10 mL of 1,1,1,3,3,3-hexafluoro-2-propanol (HFIP; Daejeong Chemical, Korea) and sonicated using a probe-type sonicator (VCX750, Vibra-Cell, USA) at 20% amplitude with 10-second on/off pulses for 10 cycles. After complete dispersion, PCL pellets were added to the UdECM solution to achieve a total solute content of 0.6 g. The mixture was continuously stirred at 200 rpm for 24 h at room temperature to obtain a homogeneous solution. The final concentration of the electrospinning solution was approximately 6% (w/v).

Fabrication of PCL/UdECM electrospun composite scaffolds

Electrospinning was carried out onto a rotating stainless-steel mandrel (diameter = 5 mm) at 500 rpm. This relatively low rotational speed was intentionally chosen to yield randomly oriented fibers, thereby providing isotropic mechanical behavior that supports uniform circumferential compliance of the tubular graft under pulsatile loading.[37] A 21G metal needle (NanoNC, Korea) was positioned at a spinneret-to-collector distance (SCD) of 10 cm (100 mm) from the mandrel and polymer solutions were electrospun under an applied voltage of 10 kV at a feed rate of 0.08 mL h^{-1} for 2 h. The temperature and relative humidity were maintained at 25 °C and 35%, respectively, by the laboratory air-conditioning system. To decouple processing from composition, the SCD, applied voltage, and feed rate were kept constant across all experiments. Standardization of flight time, solvent evaporation, and charge dissipation ensured that differences in fiber morphology could be attributed primarily to UdECM content rather than process variations. Freshly prepared solutions were used within 24 h of mixing, and needles were routinely replaced to prevent tip fouling. Each composition was fabricated in three independent batches for downstream analyses. After electrospinning, chemical crosslinking was performed by immersing the scaffolds in 50 mL of 99% ET-OH containing 100 mM EDC/NHS at 4 °C for 4 h. The scaffolds were then rinsed with ET-OH and deionized water at 4 °C for 1 h to remove residual crosslinkers. To facilitate scaffold removal without damaging the fibers, the mandrel was incubated in 20% (w/v) Pluronic® F-127 for 30 min at 4 °C, then allowed to gel at room temperature for an additional 30 min, and finally placed in a 37 °C water bath for 15 min. Residual Pluronic® F-127 was removed by washing in triple-distilled water at 4 °C for 2 days. The resulting scaffolds were freeze-dried for 48 h and stored at −80 °C until further analysis.

Fourier transform infrared spectroscopy (FTIR)

FTIR (Nicolet iS10, Thermo Fisher Scientific, Madison, WI, USA) was conducted to verify the incorporation of UdECM within the

Table 1 Composition of electrospinning solutions prepared with varying ratios of PCL and UdECM in HFIP

	PCL (g)	UdECM (g)	HFIP (mL)	Final concentration (w/v%)
Pure PCL	0.6	0	10	6
PCL/UdECM-1	0.594	0.006	10	6
PCL/UdECM-5	0.57	0.03	10	6
PCL/UdECM-10	0.54	0.06	10	6

electrospun scaffolds. Samples included PCL-only controls and PCL/UdECM composites containing 1, 5, and 10 wt% UdECM. Spectral data were acquired in the 600–4000 cm^{-1} range at a resolution of 4 cm^{-1}, and the average of 30 scans was used for analysis.

Water contact angle measurement

The hydrophilicity of the electrospun scaffolds was assessed *via* water contact angle measurements. Scaffolds were cut into 8 × 8 mm^2 squares, and a 10 μL droplet of Rhodamine B solution (Sigma-Aldrich, USA) was gently placed on each sample surface. Contact angles were recorded at 0, 5, 10, 15, and 20 seconds and analyzed using ImageJ software. Data are presented as mean ± standard deviation ($n = 4$).

Water absorption test

The water absorption capacity of the scaffolds was examined by immersing 8 × 8 mm^2 samples in distilled water at 37 °C for 2 h. After immersion, the samples were lightly blotted to remove excess water and weighed immediately. The water absorption (%) was calculated using the following equation:

$$\text{Water Absorption (\%)} = W_t - W_0/W_0 \times 100$$

where W_t is the wet sample weight and W_0 is the initial dry sample weight ($n = 4$).

Mechanical testing

The mechanical properties of electrospun scaffolds were evaluated using a universal testing machine (UTM; Top-tech 2000, Chemilab, Suwon, South Korea). For tensile testing, samples were cut into rectangular strips with dimensions of 4 × 8^2 mm. The tensile strength and Young's modulus were measured using a 10 kgf load cell at a constant extension rate of 5 mm min^{-1}. Young's modulus was calculated from the slope of the linear region of the stress–strain curve. All experiments were conducted in quadruplicate, and results are expressed as mean ± standard deviation ($n = 3$).

Scanning electron microscopy (SEM)

Fiber morphology was observed by SEM (SNE-3000 M, SEC Inc., South Korea) at an accelerating voltage of 10 kV. Samples were sputter-coated with gold (thickness ~5 nm) prior to imaging. Fiber diameter was measured using ImageJ software for at least 60 fibers per sample, and the data are reported as mean ± standard deviation ($n = 60$).

In vitro cell culture

To evaluate cytocompatibility, EA.hy926 human vascular endothelial cells (ATCC, USA) were cultured in Dulbecco's Modified Eagle's Medium-High Glucose (DMEM-H, Sigma-Aldrich, USA) supplemented with 10% fetal bovine serum (FBS, Thermo Fisher Scientific, USA) and 1% penicillin–streptomycin (P/S, Thermo Fisher Scientific, USA). Cells were cultured at 37 °C in a 5% CO_2 incubator, with medium changes every 2 days.

Assessment of cell viability and proliferation

Scaffolds (8 × 8 mm^2) were seeded with EA.hy926 endothelial cells at a density of 5 × 10^4 cells per scaffold and incubated for 1 and 7 days. Live cells were stained with 0.15 mM Calcein AM (Invitrogen, USA) and dead cells with 2 mM Ethidium Homodimer-1 (Invitrogen, USA), and the resulting fluorescence images were captured by a confocal laser scanning microscope (LSM700, Carl Zeiss, Germany). To visualize cell morphology and cytoskeletal organization, samples were further cultured for 3 and 14 days, fixed in 3.7% paraformaldehyde, permeabilized in 0.1% Triton X-100, and stained with DAPI (1 : 10 000) and Alexa Fluor™ 488 Phalloidin (1 : 100), after which confocal microscopy (LSM700) was used for imaging. Cell proliferation on scaffolds (8 × 8 mm^2) was quantified at days 1, 3, and 7 *via* the MTT proliferation assay (Roche, USA), according to the manufacturer's instructions, with each condition tested in quadruplicate ($n = 4$) and data presented as mean ± standard deviation.

Tube formation assay

An *in vitro* tube formation assay was performed to evaluate the angiogenic potential of the scaffolds. Matrigel® (100 μL per well; Corning, USA) was added to 24-well cell culture plates and allowed to polymerize at 37 °C for 30 min. EA.hy926 cells (5 × 10^4 cells per well) were seeded onto the solidified Matrigel, and scaffolds were placed in Transwell inserts positioned above the cell layer. After 6 hours of incubation at 37 °C in a 5% CO_2 atmosphere, tube formation was observed by optical microscopy. Images captured at 2 and 6 hours were analyzed using ImageJ software to quantify the number of junctions and total tube length per field. All experiments were conducted in triplicate ($n = 3$).

In vitro coagulation assay

The anticoagulant properties of the scaffolds were tested using an *in vitro* coagulation assay. Scaffolds (8 × 8 mm^2) were prepared using a biopsy punch and placed in 24-well plates. Fresh rat whole blood (200 μL) gently applied to each disc and incubated at 37 °C for 5 minutes. Subsequently, 500 μL of distilled water were carefully added to lyse non-coagulated blood. After 10 minutes of stabilization, the supernatant was collected and transferred to a 96-well plate. Absorbance was measured at 450 nm using a microplate reader. All experiments were conducted in quadruplicate, and results are expressed as mean ± standard deviation ($n = 4$).

Blood cell adhesion assay

Adhesion of blood components on scaffold surfaces was evaluated using fresh rat whole blood. Scaffolds were cut into 8 × 8 mm^2 pieces and placed in 24-well plates. A volume of 200 μL of fresh whole blood was pipetted onto each sample and incubated at 37 °C for 30 minutes. Samples were subsequently washed three times with PBS to remove non-adherent cells and fixed in 2.5% glutaraldehyde for 2 hours at room temperature. Dehydration was carried out through a graded ethanol series (50%,

60%, 70%, 80%, 90%, and 100%). After drying, the scaffold surfaces were examined by scanning electron microscopy (SEM; SNE-3000M, SEC Inc., South Korea) to assess blood cell attachment and morphology ($n = 4$).

Statistical analysis

All data are presented as mean ± standard deviation (SD). Statistical analyses were performed using SPSS software (SPSS, Inc., USA). A Student's *t*-test was used to compare two groups, while one-way analysis of variance (ANOVA) followed by Tukey's honest significant difference (HSD) post hoc test was applied for comparisons among three or more groups. *p*-values of < 0.05 (*), < 0.01 (**), and < 0.001 (***) were considered statistically significant.

Results and discussion

Characterization of decellularized *Urechis unicinctus* ECM (UdECM)

To evaluate the potential of extracellular matrix derived from *Urechis unicinctus* (UdECM) as a bioactive component for vascular tissue engineering, we performed a comprehensive characterization of its biochemical composition and decellularization efficiency (Fig. 1). A macroscopic comparison of the native body wall and decellularized UdECM revealed the successful removal of pigmented cellular components, resulting in a translucent, whitish ECM (Fig. 1(b)). This visible change indicates effective decellularization while preserving the tissue's overall structural integrity.[27]

SDS-PAGE analysis showed distinct protein bands ranging from approximately 120 to 30 kDa (Fig. 1(b)), suggesting that multiple ECM-associated proteins were retained post-decellularization. In particular, the prominent band at ~120 kDa likely corresponds to intact type I collagen chains, while the lower molecular weight bands may represent collagen degradation fragments, glycoproteins, or matrix-associated peptides.[38,39] The preservation of these protein profiles indicates that essential structural and bioactive ECM components remained largely intact following decellularization.

Quantitative DNA analysis confirmed the efficient removal of cellular nucleic acids, with residual DNA levels reduced to 26.06 ± 0.94 ng mg^{-1} of dry tissue well below the widely accepted threshold of 50 ng mg^{-1} thereby minimizing the risk of immunogenicity in downstream applications (Fig. 1(c)).[40] Biochemical assays further showed the retention of key ECM macromolecules, including total collagen (121.16 ± 2.47 μg mg^{-1} *vs.* native:143.13 ± 6.86 μg mg^{-1}), GAGs (24.11 ± 0.32 μg mg^{-1} *vs.* native: 45.56 ± 2.24 μg mg^{-1}), and elastin (128.67 ± 10.34 μg mg^{-1} *vs.* native: 56.82 ± 7.02 μg mg^{-1}) (Fig. 1(d)–(f)). Collagen provides tensile strength and structural integrity, whereas GAGs facilitate matrix hydration, growth factor retention, and cell-matrix interactions. In particular, the substantial retention of elastin is particularly advantageous for vascular applications, where elastic recoil and compliance are crucial for proper hemodynamic function.[41,42]

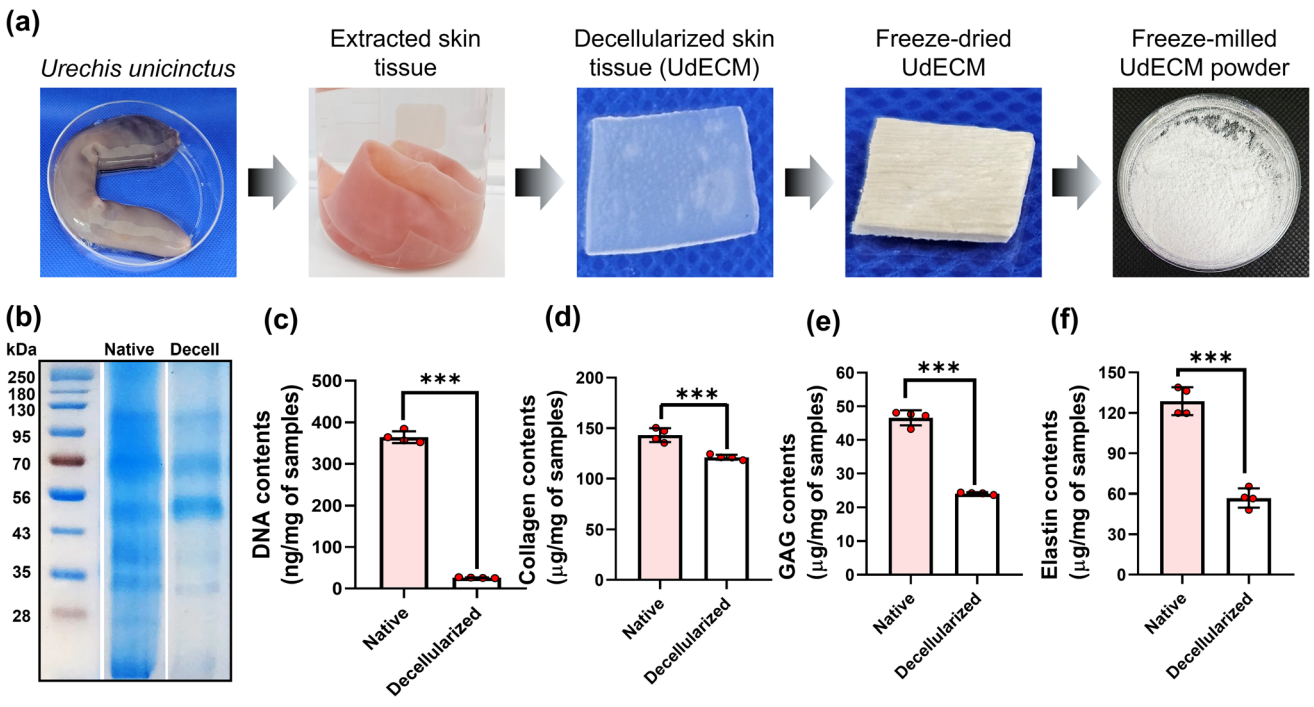

Fig. 1 Preparation and characterization of decellularized extracellular matrix (UdECM) derived from *Urechis unicinctus*. (a) Decellularization process of *Urechis unicinctus* body wall, yielding translucent UdECM, followed by freeze-drying and milling. (b) SDS-PAGE analysis comparing protein profiles between native and decellularized tissues. (c–f) Quantitative biochemical assays of ECM components in native and decellularized samples: (c) DNA content ($n = 4$), (d) collagen content ($n = 4$), (e) glycosaminoglycan (GAG) content ($n = 4$), and (f) elastin content ($n = 4$). All values represent mean ± SD. Statistical significance was determined using Student's *t*-test. *p*-values of < 0.05 (*), < 0.01 (**), and < 0.001 (***) were considered statistically significant.

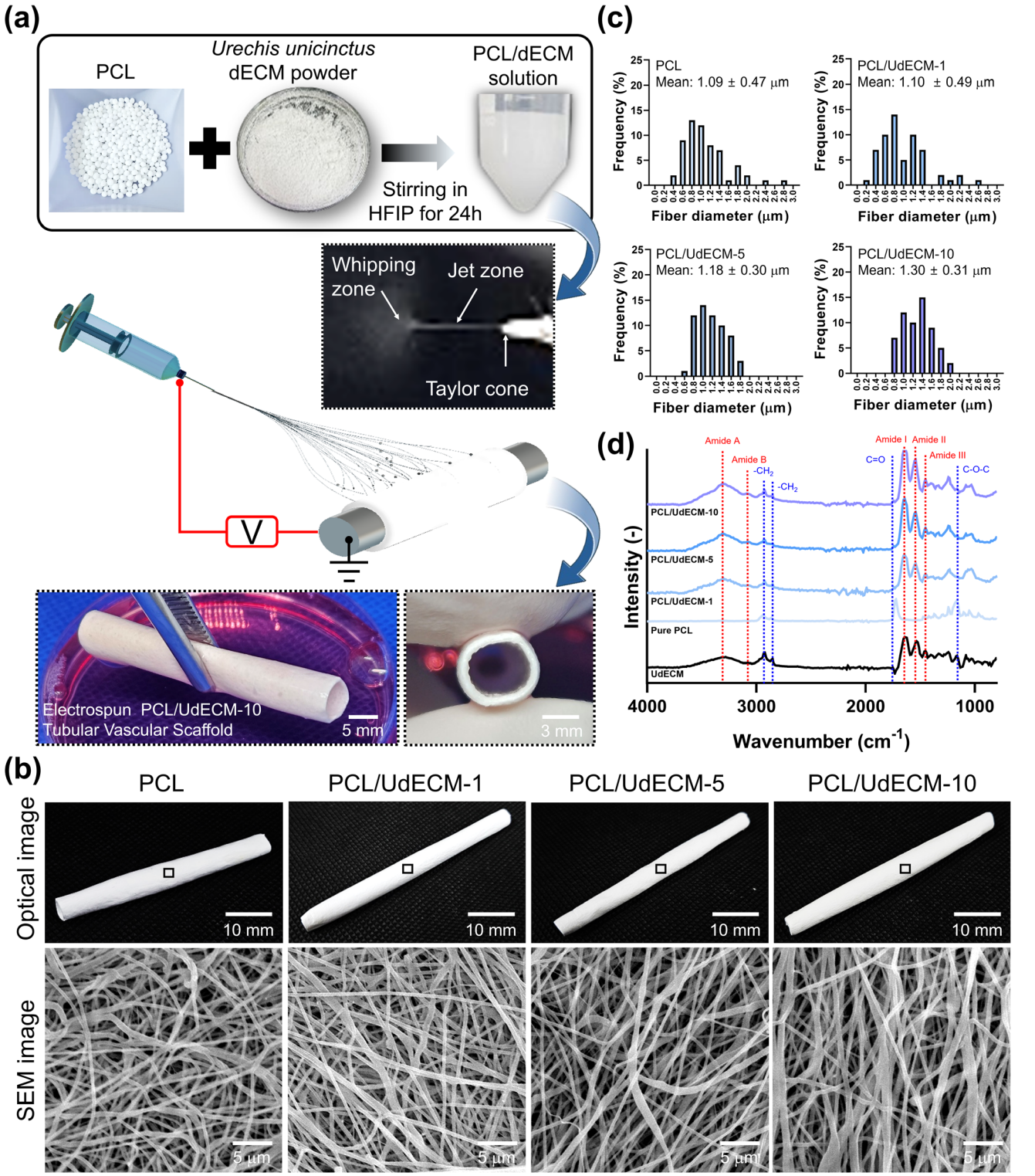

Fig. 2 Fabrication and characterization of electrospun PCL/UdECM composite vascular grafts. (a) Schematic overview of the electrospinning process, from preparing the PCL/UdECM solution to fabricating a tubular vascular scaffold. (b) Optical and SEM images of pure PCL, PCL/UdECM-1, PCL/UdECM-5, and PCL/UdECM-10 composite scaffolds. Scale bars: optical images = 10 mm; SEM images = 5 μm. (c) Fiber diameter distribution (n = 60 fibers per group, analyzed by ImageJ) of electrospun scaffolds; the average fiber diameters are indicated (mean ± SD). (d) FTIR spectra showing characteristic PCL peaks and emerging amide bands (Amide I, II, III) as UdECM is incorporated.

Although some loss of ECM components is expected during decellularization, the preserved levels appeared sufficient to maintain both mechanical integrity and biological functionality. Collectively, these findings indicate that the decellularization protocol effectively removes immunogenic material while retaining a broad spectrum of functional matrix

constituents. These attributes underscore the potential of UdECM as a biologically active additive for improving the performance of synthetic polymer-based vascular graft scaffolds.

Fabrication and characterization of electrospun PCL/UdECM scaffolds

Fig. 2(a) illustrates the fabrication process of electrospun PCL/UdECM tubular scaffolds. UdECM powder was homogeneously dispersed in HFIP with PCL under continuous stirring for 24 hours, followed by electrospinning onto a rotating mandrel to form cylindrical structures (Fig. S1). The schematic shows the formation of the Taylor cone, jet stretching, and whipping zones, ultimately generating uniform fibers deposited onto the collector. Representative photographs (bottom insets, Fig. 2(a)) confirm the feasibility of producing small-diameter, vascular graft-like constructs using this approach. Because HFIP is a polar, strongly hydrogen-bond-donating, volatile solvent, it generally stabilizes the Taylor cone and accelerates jet solidification in PCL/ECM blends.[43–45] Under these constant HFIP conditions and a fixed SCD (10 cm), morphology trends observed across groups are interpreted primarily as UdECM content-dependent effects rather than solvent or distance variations.[45]

As shown in Fig. 2(b), optical images of the fabricated tubes exhibit smooth and uniform morphologies for all UdECM concentrations (0, 1, 5, and 10 wt%). SEM reveals a well-organized fibrous architecture in the pure PCL scaffold, with no bead formation and consistent fiber diameters. Upon incorporating UdECM, subtle morphological changes are observed. While the 1 wt% UdECM scaffold remains similar to pure PCL, higher UdECM concentrations (5 and 10 wt%) produce progressively thicker and homogeneous fibers. These differences likely arise from alterations in solution viscosity, surface tension, and electrospinning jet stability caused by ECM constituents such as collagen, GAGs, and elastin.[46,47] In particular, no evidence of phase separation or large aggregate formation was seen, indicating good dispersion and processability of UdECM within the PCL matrix.

Under a constant SCD (10 cm) and identical electrospinning settings, increasing UdECM loading produced a gradual rise in mean fiber diameter from 1.09 ± 0.47 μm (PCL) and 1.10 ± 0.49 μm (PCL/UdECM 1) to 1.18 ± 0.30 μm (PCL/UdECM 5) and 1.30 ± 0.31 μm (PCL/UdECM 10) while maintaining uniform, bead-free morphologies up to 10 wt% UdECM (Fig. 2(b and c)).[46,47] At 20 wt% (Fig. S3), pronounced bead formation and irregular fibers emerged, indicating composition-induced electrospinning instability and establishing 10 wt% as the practical upper limit under the present conditions. These trends are consistent with UdECM-dependent changes in effective viscosity, surface tension, and solution conductivity that modulate jet thinning and charge dissipation when process parameters are fixed.[43,45,48–51] As a limitation, we note that solution rheology and conductivity were not directly measured in this study.

Fig. 2(d) shows the Fourier transform infrared (FTIR) spectra of PCL and PCL/UdECM scaffolds. Pure PCL shows characteristic absorption peaks at 2860–2940 cm^{-1}, corresponding to the symmetric and asymmetric stretching of $-CH_2$ groups in aliphatic polyesters, and a strong carbonyl (C=O) stretching peak near 1720–1730 cm^{-1}, consistent with earlier reports on electrospun PCL fibers.[47,53,54] The broad band spanning 1100–1300 cm^{-1} is assigned to C–O stretching vibrations typical of polycaprolactone.[52] With the incorporation of UdECM, new amide peaks appear at ~1650 cm^{-1} (amide I), ~1550 cm^{-1} (amide II), and ~1230–1300 cm^{-1} (amide III), corresponding to the proteinaceous components (*e.g.*, collagen and elastin) present in the ECM.[46,47,53] In particular, additional signals emerge near ~3070 cm^{-1} and ~3300 cm^{-1}, which can be attributed to amide B and amide A, respectively these bands originate from N–H stretching vibrations and are often observed in collagen-containing scaffolds.[47,53] The progressive increase in intensity of all these amide-related peaks with rising UdECM content confirms the successful integration of ECM proteins into the PCL fiber network. Such compositional modifications suggest enhanced bioactivity and improved cell–matrix interactions, which may be advantageous for vascular tissue engineering applications that demand regenerative potential.

Hydrophilicity and mechanical properties of PCL/UdECM scaffolds

The hydrophilicity and water absorption capacity of tissue-engineered scaffolds are crucial for promoting initial cell adhesion, protein adsorption, and nutrient diffusion particularly in vascular applications that require rapid endothelialization and effective waste removal.[54] As shown in Fig. 3(a), the water contact angle measurements reveal a progressive decrease in surface hydrophobicity with increasing UdECM content, dropping from $108 \pm 2°$ (pure PCL) to $102 \pm 2°$ (PCL/UdECM-1), $92 \pm 4°$ (PCL/UdECM-5), and $78 \pm 3°$ (PCL/UdECM-10). This result is further corroborated by the water uptake data (Fig. 3(b)), where the absorption capacity rises from $354.07 \pm 15.97\%$ (PCL) to $380.54 \pm 7.72\%$ (PCL/UdECM-1), $423.86 \pm 19.94\%$ (PCL/UdECM-5), and $446.78 \pm 12.67\%$ (PCL/UdECM-10). This enhancement is attributed to both increased porosity likely promoted by the presence of ECM powder during electrospinning and the presence of polar functional groups (*e.g.*, hydroxyl, carboxyl, amide) in ECM-derived macromolecules, thereby creating a more hydrophilic fiber surface that can facilitate cell–material interactions.[55] Such a moisture-rich environment is especially beneficial for vascular grafts, where robust cell infiltration and nutrient transport are essential.

Mechanical properties such as stiffness, elasticity, and tensile strength are critical for the functional performance of vascular grafts. These scaffolds must withstand dynamic mechanical stresses, including blood pressure-induced pulsation, radial compression, and elongation, without losing their shape or structural integrity.[56] As illustrated in Fig. 3(c), PCL/UdECM tubes maintain their cylindrical shape upon compression and exhibit near-complete recovery after force removal an indication of good elasticity and shape memory. This attribute

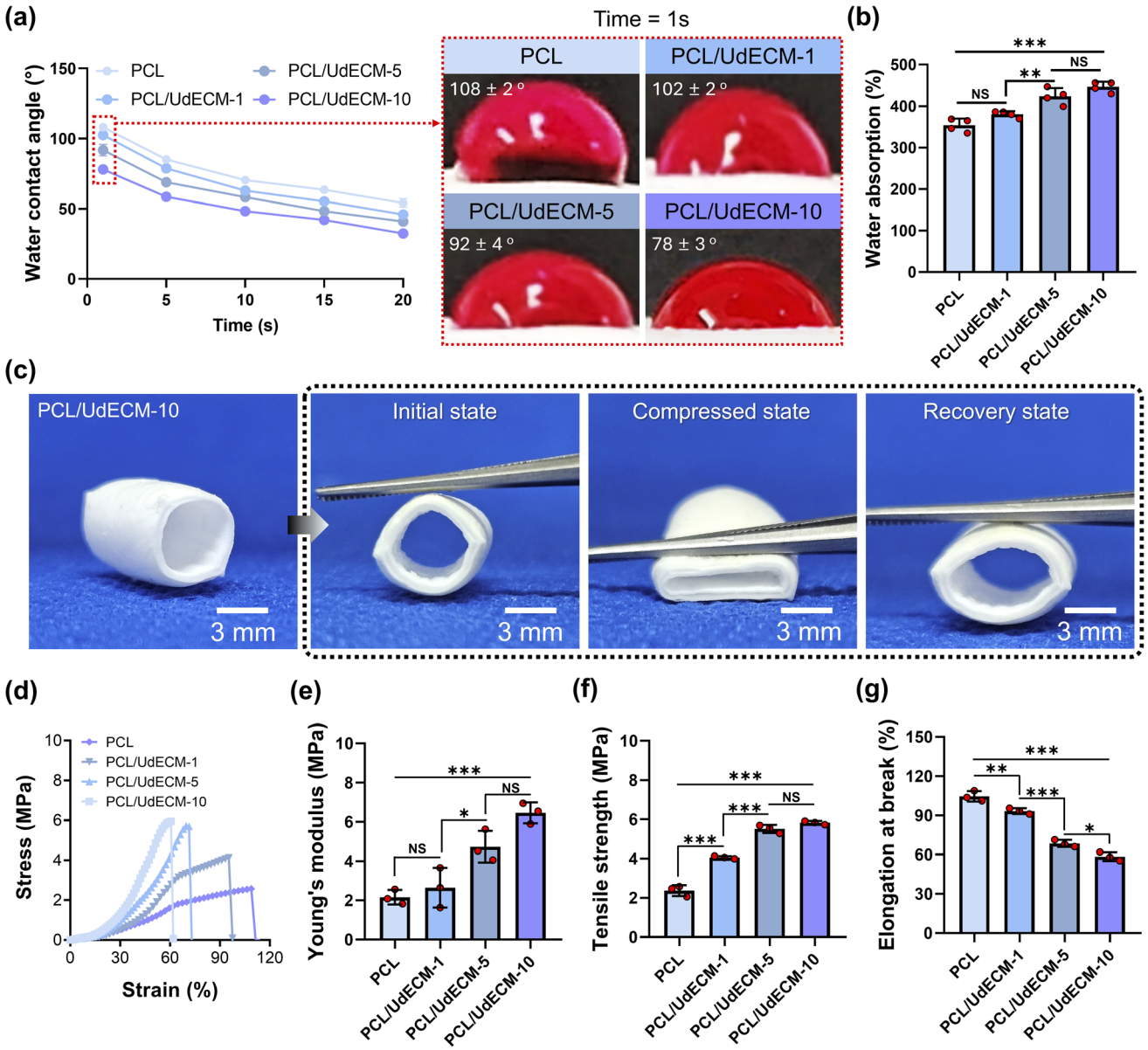

Fig. 3 Surface wettability, compressibility, and mechanical properties of PCL/UdECM composite vascular scaffolds (1, 5, and 10 wt%). (a) Time-dependent water contact angle measurements for pure PCL and PCL/UdECM composites, with inset images showing the contact angle at 1 second ($n = 4$). (b) Quantitative analysis of water absorption capacity ($n = 4$). (c) Macroscopic views of the tubular scaffolds in the initial, compressed, and recovery states. Scale bar = 3 mm. (d) Representative stress–strain curves of different scaffold compositions. (e–g) Mechanical properties of the scaffolds: (e) Young's modulus, (f) tensile strength, and (g) elongation at break ($n = 3$). All values represent mean ± SD. Statistical analysis was performed using one-way ANOVA with Tukey's post hoc test. $p < 0.05$ (*), < 0.01 (**), and < 0.001 (***); NS = not significant.

ensures that the graft can be surgically manipulated without permanent deformation and maintain patency under physiological conditions, including variable shear stress and pulsatile loading.

(Fig. 1(d)–(f)) detail the tensile properties of these tubular scaffolds. Increasing UdECM loading progressively enhances the Young's modulus, from 2.16 ± 0.37 MPa (PCL) to 2.64 ± 1.01 MPa (PCL/UdECM-1), 4.73 ± 0.80 MPa (PCL/UdECM-5), and 6.46 ± 0.54 MPa (PCL/UdECM-10), with PCL/UdECM-5 and -10 exhibiting significantly higher stiffness than pure PCL ($p <$ 0.001). A similar pattern is observed in tensile strength, which rises from 2.37 ± 0.27 MPa (PCL) to 4.06 ± 0.07 MPa (PCL/UdECM-1), 5.51 ± 0.20 MPa (PCL/UdECM-5), and 5.81 ± 0.09 MPa (PCL/UdECM-10). In particular, the difference between 5 and 10 wt% UdECM groups is not statistically significant (NS), suggesting that mechanical gains may plateau beyond 5 wt% ECM incorporation. This improvement likely arises from the reinforcing effect of structural proteins such as collagen and elastin, which enhance inter-fiber bonding and matrix cohesion through hydrogen bonding and other intermolecular interactions.[55] Furthermore, the uniform dispersion of ECM macromolecules in the polymer solution can facilitate direct molecular–level interactions between PCL chains and ECM

functional groups, strengthening the fibrous network and promoting effective load transfer.[55]

In contrast, the elongation at break decreases as UdECM concentration increases an expected trade-off between stiffness and flexibility. While pure PCL exhibits the highest ductility (104.50 ± 3.96%), the value drops to 58.36 ± 3.31% at 10 wt% UdECM. Despite this reduction, the remaining ductility is still sufficient for accommodating physiological deformations in small-diameter vessels. Thus, a balance can be struck between mechanical rigidity (for maintaining lumen integrity) and elasticity (for adapting to dynamic loading), with the optimum UdECM content potentially depending on specific surgical or physiological requirements.

Overall, these findings confirm that increasing UdECM loading not only improves the scaffold's hydrophilicity leading to enhanced water absorption and a more cell-friendly surface

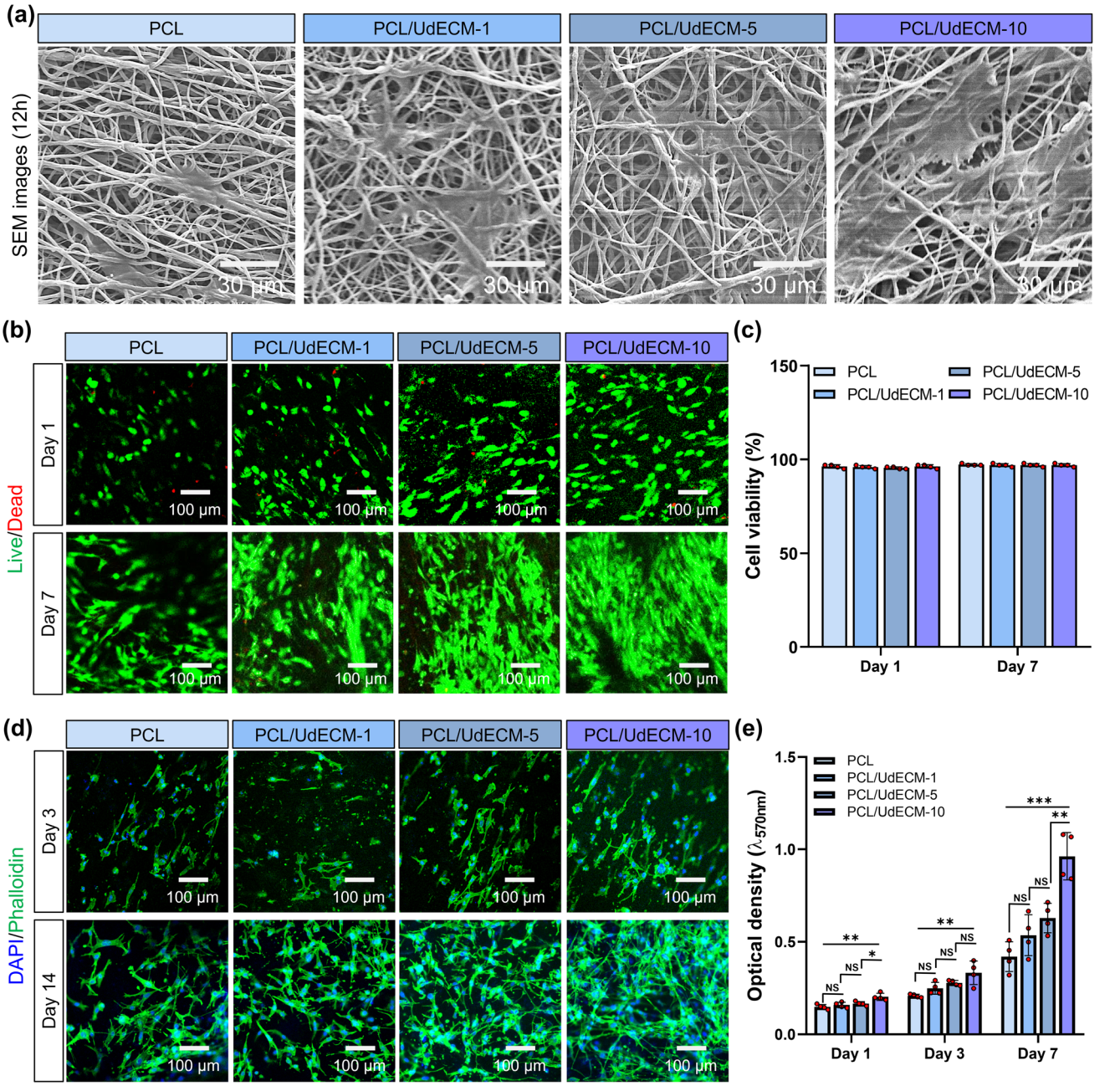

Fig. 4 *In vitro* biocompatibility and cell behavior on pure PCL and PCL/UdECM composite scaffolds (1, 5, and 10 wt%). (a) SEM images at 12 h reveal cell morphology and attachment on scaffold surfaces. Scale bar = 30 μm. (b) Live/dead staining (green/red) images of EA.hy926 cells cultured on different scaffolds at day 1 and day 7, showing high cell viability and cell attachment across all groups. Scale bar = 100 μm. (c) Quantitative cell viability measured at Day 1 and 7 ($n = 4$). (d) Cytoskeletal organization visualized by DAPI (nuclei, blue) and phalloidin (F-actin, green) staining at day 3 and day 14. Scale bar = 100 μm. (e) MTT assay results showing time-dependent cell proliferation on each scaffold ($n = 4$). All values represent mean ± SD. Statistical analysis was performed using one-way ANOVA with Tukey's post hoc test. $p < 0.05$ (*), < 0.01 (**), and < 0.001 (***); NS = not significant.

but also modulates its mechanical profile in a manner beneficial for vascular applications. Enhanced stiffness and recovery from compression help prevent graft collapse under pulsatile flow, while a moderate elongation at break allows the scaffold to adapt to physiological strains. This synergy of hydrophilic surface properties, mechanical robustness, and inter-fiber cohesion underscores the potential of PCL/UdECM tubular scaffolds for durable, small-diameter vascular grafts.

Cytocompatibility and cellular interactions on PCL/UdECM scaffolds

In vascular tissue engineering, a scaffold's ability to support cell adhesion, proliferation, and the formation of a functional endothelium is crucial for successful graft integration and long-term patency.[20,23] To evaluate these parameters, we examined electrospun PCL and PCL/UdECM scaffolds (1, 5, 10 wt%) at various time points, focusing on initial cell attachment, viability, cytoskeletal organization, and proliferation (Fig. 4).

Fig. 4(a) shows scanning electron microscopy (SEM) images taken at 12 h, providing insights into early cell adhesion and spreading. On pure PCL, cells appear primarily atop individual fibers with limited bridging between them. In contrast, PCL/UdECM scaffolds (1, 5, 10 wt%) display more extensive coverage, with cells often spanning adjacent fibers. This enhanced early attachment could be attributed to the bioactive nature of ECM components, which improve surface hydrophilicity and offer integrin-binding sites, thereby facilitating cell-fiber.[57,58]

Live/Dead staining results Fig. 4(b) indicate that all scaffolds maintain high cell viability (>95%) at both Day 1 and Day 7, with negligible red fluorescence (dead cells). As shown quantitatively in Fig. 4(c), there are no statistically significant differences among the groups, suggesting comparable cytocompatibility in the early phase of culture. Although visually the PCL/UdECM-5 and -10 groups appear to host slightly denser cell layers by Day 7, the viability values remain similarly high across all conditions.

To assess cytoskeletal organization and cell distribution over a longer term, Fig. 4(d) presents DAPI (nuclei) and phalloidin (F-actin) staining at Days 3 and 14. By Day 3, cells on PCL/UdECM scaffolds exhibit more robust actin filament formation and a denser arrangement than those on pure PCL. This trend becomes more pronounced by Day 14, where increasing UdECM loading correlates with a well-developed monolayer and an extensive actin network. ECM-derived proteins may contribute binding motifs and optimal local stiffness, promoting stress-fiber formation and integrin clustering.[55] In contrast, cells on pure PCL remain relatively scattered, potentially due to its hydrophobic surface and fewer functional groups for direct cell adhesion.

Fig. 4(e) shows the MTT assay results, reflecting cell proliferation from Day 1 to Day 7. All scaffolds support an overall increase in cell number, yet the UdECM-containing groups (PCL/UdECM-1, -5, and -10) display higher optical density (OD) values than pure PCL at each time point. In particular, PCL/UdECM-10 exhibits the greatest OD on Day 7, showing a statistically significant ($p < 0.001$) difference from pure PCL. This suggests that a higher UdECM content may provide additional bioactive cues such as integrin-recognition motifs or growth-factor binding domains to further enhance cell growth.[59] Nonetheless, the differences among UdECM groups (1, 5, 10 wt%) may depend on specific cell types or extended culture durations, warranting further optimization. Furthermore, EDC/NHS crosslinking can stabilize the PCL/UdECM scaffolds by reducing enzymatic degradation and enhancing resistance to hydrolytic breakdown, thereby supporting long-term biocompatibility. At the same time, prior studies on collagen matrices have indicated that carbodiimide crosslinking may modify integrin-binding carboxyl groups, which could subtly alter native-like cell-ECM recognition while still permitting favorable cytocompatibility.[60]

Collectively, these findings confirm that incorporating UdECM into PCL scaffolds preserves excellent cytocompatibility while improving early cell attachment, promoting robust cytoskeletal organization, and enhancing proliferation over time. In particular, increasing UdECM loading correlates with a more extensive actin network and well-organized cell monolayer by Day 14, which are important for vascular applications requiring a stable endothelial lining. Future studies will focus on optimizing UdECM concentration and investigating long-term functionality *in vivo* to fully harness the potential of PCL/UdECM scaffolds for small-diameter vascular grafts.

In vitro endothelial tube formation

Rapid and robust endothelialization is essential for successful vascular graft integration and the formation of functional microvasculature in tissue-engineered constructs.[23] Fig. 5(a) provides a schematic overview of the sequential transitions (cell attachment, cluster formation, cell sprouting, and tube formation) during the 6-hour incubation. To evaluate the angiogenic potential of PCL/UdECM scaffolds, we performed an *in vitro* endothelial tube formation assay using EA.hy926 cells (5×10^4 cells per well) (Fig. 5(b)–(e)).

Fig. 5(b) shows representative optical images at 2 h and 6 h. In the pure PCL group, cells remain mostly as single cells or very loosely arranged at 2 h, showing minimal extension into interconnected structures by 6 h. Likewise, PCL/UdECM-1 does not exhibit notable cluster formation early on, although cells appear more adherent compared to pure PCL. In contrast, PCL/UdECM-5 and PCL/UdECM-10 support more pronounced cluster-like arrangements and cell sprouting as early as 2 h, forming extensive capillary-like networks by 6 h. These morphological differences suggest that ECM-derived components facilitate cohesive cell assembly and network maturation over time.

Fig. 5(c)–(e) show the quantitative results of the tube formation assay, including the number of junctions, tubes, and total tube length per field at 2 and 6 hours. As UdECM loading increases, overall angiogenic metrics improve. While PCL/UdECM-1 shows a modest yet statistically significant rise ($p < 0.05$) in junction formation at 2 h, PCL/UdECM-5 and PCL/UdECM-10 further enhance both the number of connections and total tube length ($p < 0.01$ or 0.001). By 6 h, the differences

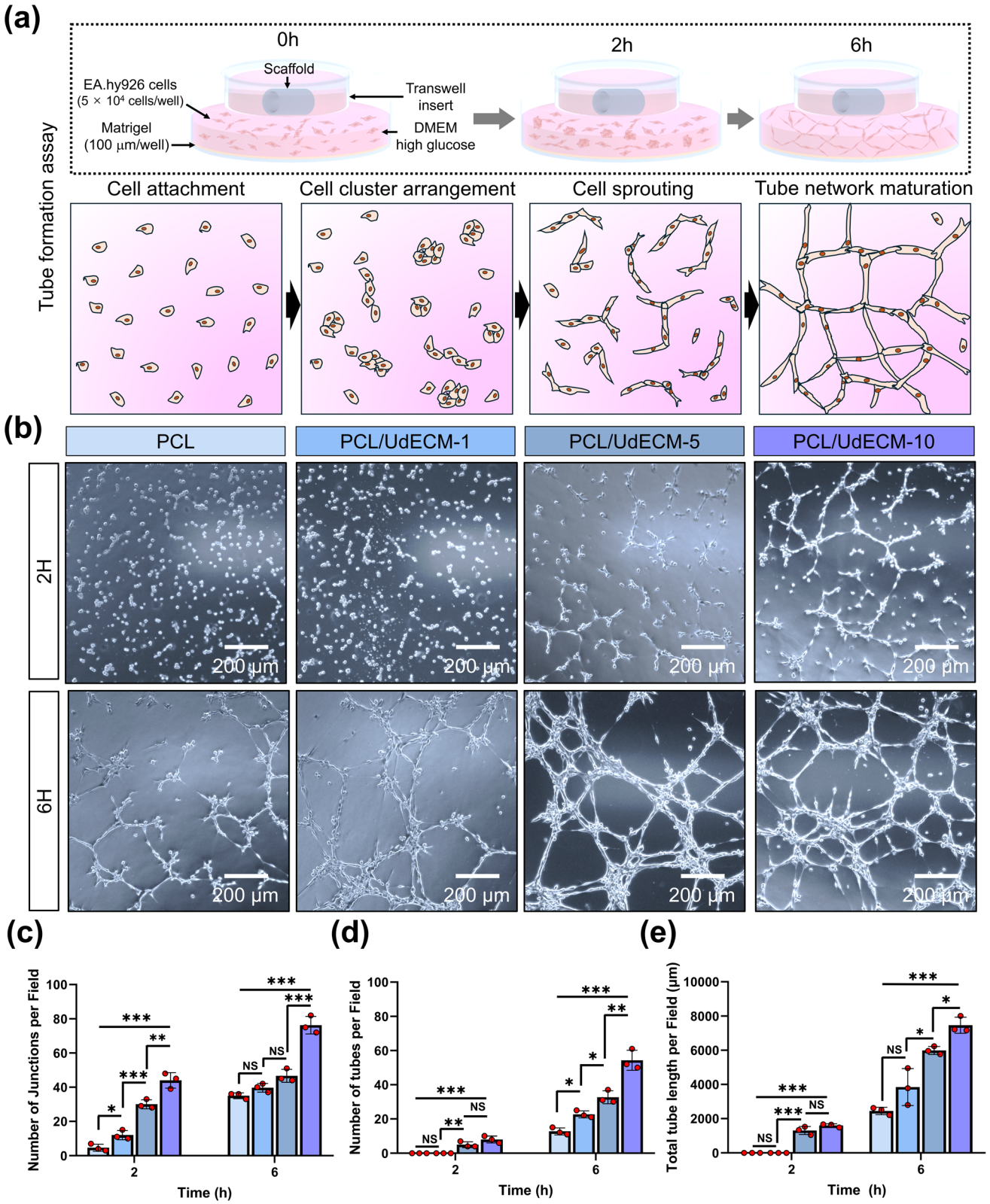

Fig. 5 Proangiogenic potential of PCL/UdECM composite scaffolds evaluated by *in vitro* tube formation assay. (a) Schematic illustration of the tube formation assay setup and the typical progression stages of endothelial tube formation: cell attachment, cluster arrangement, sprouting, and network maturation. EA.hy926 endothelial cells (5×10^4 cells per well) were seeded on Matrigel, and scaffolds were placed in Transwell inserts positioned above the cell layer. (b) Representative optical images of EA.hy926 cells cultured on different scaffolds (pure PCL and PCL/UdECM-1, -5, and -10) at 2 and 6 hours, showing enhanced tube formation with increasing UdECM content. Scale bar = 200 μm. (c–e) Quantitative analysis of angiogenic parameters at each time point: (c) number of junctions per field ($n = 3$), (d) number of tubes per field ($n = 3$), and (e) total tube length per field ($n = 3$). All values represent mean ± SD. Statistical analysis was performed using one-way ANOVA with Tukey's post hoc test. $p < 0.05$ (*), < 0.01 (**), and < 0.001 (***); NS = not significant.

among groups become more pronounced, with PCL/UdECM-10 displaying the highest values across all metrics ($p < 0.001$ *vs.* pure PCL). This result indicates that sufficiently high UdECM content can induce robust tube formation, in line with the morphological findings in Fig. 5(b).

These findings align with the hypothesis that ECM-derived bioactive cues enhance endothelial cell adhesion and migration critical factors for network assembly and stabilization. The incorporation of ECM proteins can facilitate integrin-mediated binding, improve local cell-to-cell interactions, and potentially modulate signaling pathways related to angiogenesis (*e.g.*, VEGF, FGF).[61] Consequently, the presence of UdECM likely lowers the activation barrier for cells to form stable junctions and elongate into tube-like structures.

Moreover, the stark contrast between pure PCL and UdECM-containing groups highlights the significance of bioactive surface modification in vascular applications. While pure PCL provides a baseline scaffold, its relatively inert nature can hinder the early stages of angiogenic network development. By introducing UdECM at concentrations of 5–10 wt%, we observe a more physiologically relevant microenvironment, in which endothelial cells can readily attach, cluster, and extend tubular structures.

Hemocompatibility and anticoagulant activity

In vascular graft applications, hemocompatibility the ability to minimize thrombus formation and blood cell adhesion is a critical factor influencing long-term patency and clinical success.[62] Fig. 6 shows the interaction of whole blood with PCL and PCL/UdECM (1, 5, and 10) scaffolds, providing insights into their anticoagulant properties and hemocompatibility. As shown in Fig. 6(a), 200 μL of fresh blood was deposited onto each scaffold, followed by a gentle rinse with water. The collected rinsing water was then visually inspected. Pure PCL

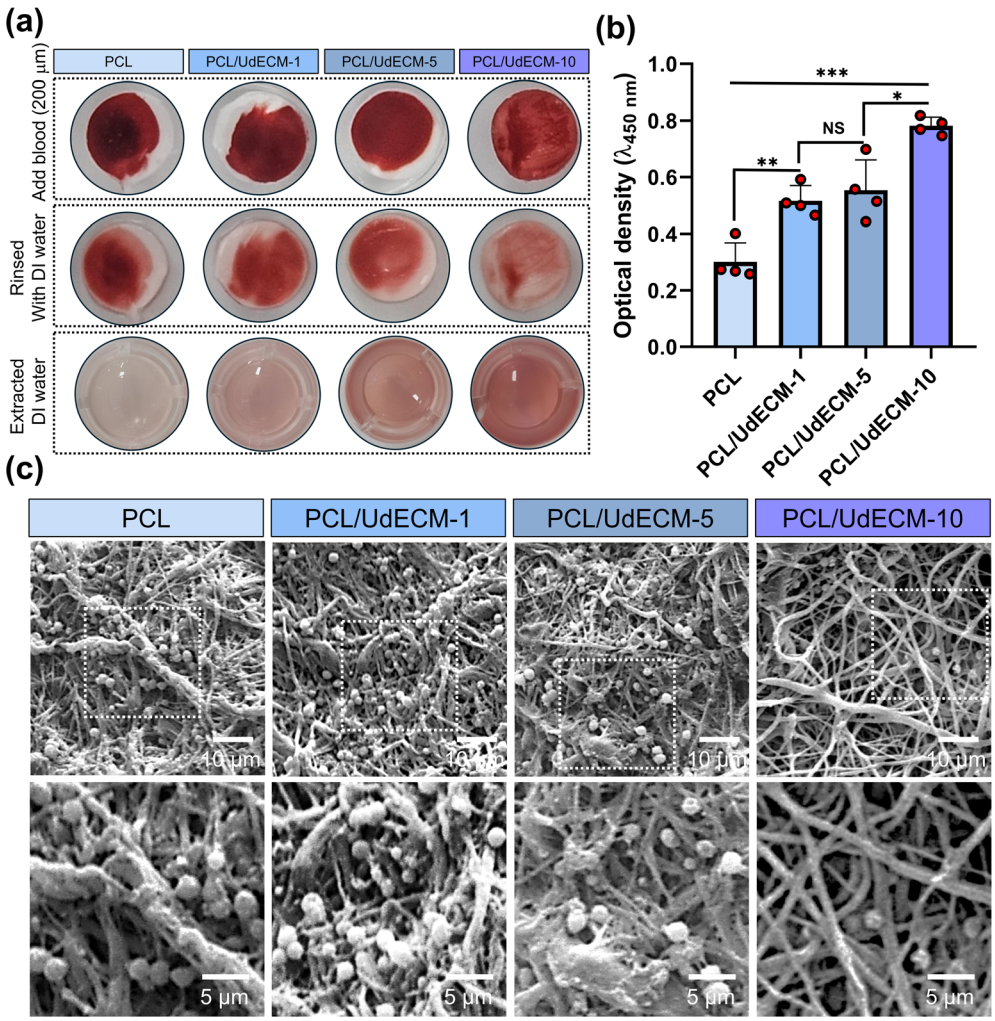

Fig. 6 Hemocompatibility and morphological evaluation of blood (200 μL) interactions on pure PCL and PCL/UdECM composite scaffolds (1, 5, and 10 wt%). (a) Visual assessment of whole blood retention, rinsing, and DI water extraction from scaffolds with increasing UdECM content, showing differences in hemoadsorption behavior. (b) Quantitative analysis of blood retention by optical density measurement at 450 nm after DI water extraction ($n = 4$). (c) SEM images of blood-treated scaffolds reveal platelet/RBC adhesion and distribution patterns. Scale bars: top panel = 10 μm; bottom panel = 5 μm. All values represent mean ± SD. Statistical analysis was performed using one-way ANOVA with Tukey's post hoc test. $p < 0.05$ (*), < 0.01 (**), and < 0.001 (***); NS = not significant.

appeared to retain most of the blood on its surface, rendering the extracted water relatively clear. In contrast, PCL/UdECM-10 scaffold produced a deeper red-colored rinsate, implying fewer red blood cells (RBCs) remained adhered to the scaffold and more RBCs stayed in suspension.

To quantify these observations, the OD of the extracted solutions was measured Fig. 6(b). PCL/UdECM-10 displayed the highest OD (0.78 ± 0.03), followed by PCL/UdECM-5 (0.55 ± 0.11) and PCL/UdECM-1 (0.52 ± 0.05). In contrast, pure PCL recorded the lowest OD (0.30 ± 0.07). The higher UdECM content correlated with significantly elevated OD values ($p <$ 0.05 or 0.01 or 0.001 among groups), suggesting that UdECM-containing scaffolds exhibit anticoagulant or anti-adhesive effects, preventing extensive RBC clotting or fiber adhesion. As a result, a greater fraction of RBCs remained unbound, leading to higher hemoglobin concentrations in the rinsate. This finding aligns with previous reports demonstrating the anticoagulant properties of glycosaminoglycans (GAGs) and other bioactive components in marine-derived ECM.[33,35]

Representative SEM images of the scaffold surfaces after blood contact Fig. 6(c) further support these findings. On pure PCL, aggregated RBCs are visibly enmeshed within the fibrous matrix, suggesting pronounced cell adhesion and the potential onset of clot formation. Conversely, PCL/UdECM-10 displays fewer large RBC clusters, with cells appearing more loosely attached or even absent in certain areas. This reduced cell accumulation may be attributed to the presence of collagen-like proteins and GAGs, which modulate local protein adsorption and minimize platelet/RBC adhesion.[63,64] Such surface characteristics are especially relevant for small-diameter vascular grafts, where thrombus formation critically affects patency.

Conclusion

In this study, we developed and characterized novel electrospun polycaprolactone (PCL)/*Urechis unicinctus*-derived extracellular matrix (UdECM) composite scaffolds for small-diameter vascular graft applications. Decellularization of *U. unicinctus* body wall yielded an ECM rich in collagen, GAGs, and elastin, with minimal residual DNA content, ensuring low immunogenic risk. These findings demonstrated that incorporating UdECM (1, 5, and 10 wt%) into PCL yields concentration-dependent improvements in scaffold hydrophilicity, mechanical properties (stiffness and tensile strength), and cytocompatibility. In particular, the PCL/UdECM-10 scaffold supported higher endothelial cell viability, enhanced proliferation, and more robust tube formation compared to pure PCL. Hemocompatibility tests further revealed that increased UdECM content conferred beneficial anticoagulant and antithrombotic effects by reducing red blood cell adhesion and clot formation. Although these results confirm excellent *in vitro* performance, further *in vivo* studies such as small-animal arterial implantation are needed to evaluate long-term biocompatibility, hemocompatibility, immunomodulation, and scaffold degradation under physiological conditions. Direct comparison with recently developed TEVGs would also be valuable to benchmark translational potential. Nevertheless, by combining the robust mechanics of PCL with the bioactive, elastin- and GAG-rich composition of UdECM, this work establishes a foundation for advancing marine-sourced ECM as a novel biomaterial in vascular tissue engineering and broader regenerative medicine applications.

Author contributions

Jong Won Mun: conceptualization, methodology, data curation, writing – original draft. Seung Pil Pack: investigation, methodology, funding acquisition. Hyeongjin Lee: conceptualization, methodology, funding acquisition, supervision, writing – review & editing. The manuscript was prepared with contributions from all authors, and all authors have approved the final version.

Conflicts of interest

The authors declare that they have no competing interests.

Data availability

Supplementary information: All data supporting this study are provided in the manuscript and SI or are available from the corresponding author upon reasonable request. See DOI: **https://doi.org/10.1039/d5ra04406e**.

Acknowledgements

This research was supported by Korea University Grant and Basic Science Research Program through the National Research Foundation of Korea (NRF) funded by the Ministry of Education (No. RS-2023-00249119). Additionally, this research was supported by NRF grants funded by the Korean government (MSIT; Ministry of Science and ICT) (No. RS-2021-NR060107).

References

1 L. West-Livingston, J. W. Lim and S. J. Lee, Translational tissue-engineered vascular grafts: from bench to bedside, *Biomaterials*, 2023, **302**, 122322.
2 L. E. Niklason and J. H. Lawson, Bioengineered human blood vessels, *Science*, 2020, **370**, 6513.
3 R. D. Kirkton, M. Santiago-Maysonet, J. H. Lawson, W. E. Tente, S. L. M. Dahl, L. E. Niklason and H. L. Prichard, Bioengineered human acellular vessels recellularize and evolve into living blood vessels after human implantation, *Sci. Transl. Med.*, 2019, **11**, 485.
4 K. W. Lee, P. S. Gade, L. Dong, Z. Zhang, A. M. Aral, J. Gao, X. Ding, C. E. T. Stowell, M. U. Nisar, K. Kim, D. P. Reinhardt, M. G. Solari, V. S. Gorantla, A. M. Robertson and Y. Wang, A biodegradable synthetic graft for small arteries matches the performance of autologous vein in rat carotid arteries, *Biomaterials*, 2018, **181**, 67–80.
5 Z. Liu, C. Tang, N. Han, Z. Jiang, X. Liang, S. Wang, Q. Hu, C. Xiong, S. Yao, Z. Wang, Z. L. Wang, D. Zou and L. Li,

Electronic vascular conduit for *in situ* identification of hemadostenosis and thrombosis in small animals and nonhuman primates, *Nat. Commun.*, 2025, **16**, 2671.
6 D. P. Taggart, U. Benedetto, S. Gerry, D. G. Altman, A. M. Gray, B. Lees, M. Gaudino, *et al.*, Bilateral *versus* single internal-thoracic-artery grafts at 10 years, *N. Engl. J. Med.*, 2019, **380**, 437–446.
7 S. Pashneh-Tala, S. MacNeil and F. Claeyssens, The tissue-engineered vascular graft—past, present, and future, *Tissue Eng., Part B*, 2016, **22**, 68–100.
8 B. Ratner, Vascular grafts: technology success/technology failure, *BME Front.*, 2023, **4**, 0003.
9 W. Ye, M. Liu, Q. Li and M. Zhao, Experimental and numerical study of a novel inbuilt helical ridge small-caliber graft for artery bypass surgery, *Discover Appl. Sci.*, 2024, **6**, 561.
10 D. Hernandez-Sanchez, M. Comtois-Bona, M. Muñoz, M. Ruel, E. J. Suuronen and E. I. Alarcon, Manufacturing and validation of small-diameter vascular grafts: a mini review, *Bioact. Mater.*, 2024, **27**, 1019845.
11 S. J. Lee, J. Liu, S. H. Oh, S. Soker, A. Atala and J. J. Yoo, Development of a composite vascular scaffolding system that withstands physiological vascular conditions, *Biomaterials*, 2008, **29**, 2891–2898.
12 L. Yuan, Y. Gao, Q. Wang, K. Zhu, L. Ren and X. Yuan, Construction of small-diameter vascular grafts by electrospun zwitterionic diselenide-containing poly(ester urethane)urea with enhanced endothelialization, *Acta Biomater.*, 2025, DOI: 10.1016/j.actbio.2025.02.031.
13 Y. M. Ju, J. S. Choi, A. Atala, J. J. Yoo and S. J. Lee, Bilayered scaffold for engineering cellularized blood vessels, *Biomaterials*, 2010, **31**, 4313–4321.
14 A. Abdal-hay, M. Bartnikowski, S. Hamlet and S. Ivanovski, Electrospun biphasic tubular scaffold with enhanced mechanical properties for vascular tissue engineering, *Mater. Sci. Eng., C*, 2018, **82**, 10–18.
15 H. Wu, J. Fan, C.-C. Chu and J. Wu, Electrospinning of small diameter 3-D nanofibrous tubular scaffolds with controllable nanofiber orientations for vascular grafts, *J. Mater. Sci. Mater. Med.*, 2010, **21**, 3207–3215.
16 J. Wang, M. Xu, H. Liu, D. Wang, H. Zhang, Z. Xu, X. Shi, X. Liu and Z. Tan, Vascular grafts with a mimetic microenvironment extracted from extracellular matrix of adipocytes can promote endothelialization *in vivo*, *Acta Biomater.*, 2025, **198**, 49–62.
17 Z. Xiang, Y. Xiang, Y. Li, J. Zhang, C. Zhou, H. Yan, D. Fu and Y. Wang, Hierarchical biomimetic electrospun vascular grafts for improved patency and regeneration, *Adv. Funct. Mater.*, 2025, **35**(31), 2424981.
18 Y. Hui, J. Mao, M. Rui, Y. Huang, X. Jiang, Y. Xu, W. Wang, J. Wu, L. Zhou, K. Xi, L. Huang and L. Chen, Hydrogel microsphere-encapsulated bimetallic nanozyme for promoting diabetic bone regeneration *via* glucose consumption and ROS scavenging, *Adv. Healthcare Mater.*, 2024, **13**, 2402596.
19 S. Ozdemir, J. Oztemur, H. Sezgin and I. Yalcin-Enis, Optimization of electrospun bilayer vascular grafts through assessment of the mechanical properties of monolayers, *ACS Biomater. Sci. Eng.*, 2024, **10**, 960–974.
20 J. O. Jeong, Y. M. Ju, H. W. Kang, A. Atala, J. J. Yoo and S. J. Lee, Biofunctionalized electrospun vascular scaffolds for enhanced antithrombotic properties and *in situ* endothelialization, *ACS Appl. Mater. Interfaces*, 2023, **15**, 52313–52323.
21 S. Homaeigohar and A. R. Boccaccini, Nature-derived and synthetic additives to poly(ε-caprolactone) nanofibrous systems for biomedicine: an updated overview, *Front. Chem.*, 2022, **9**, 809676.
22 I. C. P. Rodrigues, E. S. N. Lopes, K. D. Pereira, S. C. Huber, A. L. Jardini, J. M. Annichino-Bizzacchi, A. D. Luchessi and L. P. Gabriel, Extracellular matrix-derived and low-cost proteins to improve polyurethane-based scaffolds for vascular grafts, *Sci. Rep.*, 2022, **12**, 5230.
23 Y. Xing, Y. Gu, L. Guo, J. Guo, Z. Xu and Y. Xiao, Gelatin coating promotes *in situ* endothelialization of electrospun polycaprolactone vascular grafts, *J. Biomater. Sci. Polym. Ed.*, 2021, **32**, 1161–1181.
24 L. Yang, X. Wang, M. Xiong, X. Liu, S. Luo, J. Luo and Y. Wang, Electrospun silk fibroin/fibrin vascular scaffold with superior mechanical properties and biocompatibility for applications in tissue engineering, *Sci. Rep.*, 2024, **14**, 3942.
25 J. Shi, Y. Teng, D. Li, J. He, A. C. Midgley, X. Guo, X. Wang, X. Yang, S. Wang, Y. Feng, Q. Lv and S. Hou, Biomimetic tri-layered small-diameter vascular grafts with decellularized extracellular matrix promoting vascular regeneration and inhibiting thrombosis with the salidroside, *Mater. Today Bio*, 2023, **21**, 100709.
26 C. E. Schmidt and J. M. Baier, Acellular vascular tissues: natural biomaterials for tissue repair and tissue engineering, *Biomaterials*, 2000, **21**, 2215–2231.
27 H. Lee, W. Chun and G. Kim, Three-dimensional artificial skin construct bioprinted with a marine-based biocomposite, *Biomacromolecules*, 2023, **24**, 2864–2878.
28 M. Wan, W. Qin, C. Lei, Q. Li, M. Meng, M. Fang, W. Song, J. Chen, F. Tay and L. Niu, Biomaterials from the sea: future building blocks for biomedical applications, *Bioact. Mater.*, 2021, **6**, 4255–4285.
29 G. Romano, M. Almeida, A. V. Coelho, A. Cutignano, L. G. Gonçalves, E. Hansen, D. Khnykin, T. Mass, A. Ramšak, M. S. Rocha, T. H. Silva, M. Sugni, L. Ballarin and A.-M. Genevière, Biomaterials and bioactive natural products from marine invertebrates: from basic research to innovative applications, *Mar. Drugs*, 2022, **20**, 219.
30 D. J. Choi, S. M. Choi, H. Y. Kang, H.-J. Min, R. Lee, M. Ikram, F. Subhan, S. W. Jin, Y. H. Jeong, J.-Y. Kwak and S. Yoon, Bioactive fish collagen/polycaprolactone composite nanofibrous scaffolds fabricated by electrospinning for 3D cell culture, *J. Biotechnol.*, 2015, **205**, 47–58.
31 C. Park, Y.-H. Han, S.-G. Lee, K.-B. Ry, J. Oh, E. M. A. Kern, J.-K. Park and S.-J. Cho, The developmental transcriptome atlas of the spoon worm *Urechis unicinctus* (Echiurida: Annelida), *GigaScience*, 2018, **7**, giy007.

32 F. Shahidi and A. Saeid, Bioactivity of marine-derived peptides and proteins: a review, *Mar. Drugs*, 2025, **23**, 157.
33 H.-Y. Jo, W.-K. Jung and S.-K. Kim, Purification and characterization of a novel anticoagulant peptide from marine echiuroid worm, *Urechis unicinctus*, *Process Biochem.*, 2008, **43**, 179–184.
34 S. Kimura, H. Tanaka and Y.-H. Park, Annelid skin collagen: occurrence of collagen with structure of $(\alpha_1)_2\alpha_2$ in *Urechis unicinctus*, *Comp. Biochem. Physiol., Part B:Biochem. Mol. Biol.*, 1983, **75**, 681–684.
35 Q. Cui, Z. Zhao, T. Gao and C. Yuan, Effects of glycosaminoglycan from *Urechis unicinctus* on ADP-induced platelet calcium and membrane glycoprotein expressions in rats, *Acta Haematol.*, 2021, **144**, 44–47.
36 W. S. Sung, S. H. Park and D. G. Lee, Antimicrobial effect and membrane-active mechanism of Urechistachykinins, neuropeptides derived from *Urechis unicinctus*, *FEBS Lett.*, 2008, **582**, 2463–2466.
37 C. M. Vaz, S. van Tuijl, C. V. C. Bouten and F. P. T. Baaijens, Design of scaffolds for blood vessel tissue engineering using a multi-layering electrospinning technique, *Acta Biomater.*, 2005, **1**, 575–582.
38 M. Kasturi and K. S. Vasanthan, Harvesting decellularized liver extracellular matrix from rodents for 3D scaffold fabrication, *Artif. Cells, Nanomed. Biotechnol.*, 2024, **52**, 175–185.
39 N. Y. Patrawalla, N. S. Kajave, M. Z. Albanna and V. Kishore, Collagen and beyond: a comprehensive comparison of human ECM properties derived from various tissue sources for regenerative medicine applications, *J. Funct. Biomater.*, 2023, **14**, 363.
40 P. M. Crapo, T. W. Gilbert and S. F. Badylak, An overview of tissue and whole organ decellularization processes, *Biomaterials*, 2011, **32**, 3233–3243.
41 H. Vilaça-Faria, J. Noro, R. L. Reis and R. P. Pirraco, Extracellular matrix-derived materials for tissue engineering and regenerative medicine: a journey from isolation to characterization and application, *Bioact. Mater.*, 2024, **34**, 494–519.
42 D. Di Francesco, A. Pigliafreddo, S. Casarella, L. Di Nunno, D. Mantovani and F. Boccafoschi, Biological materials for tissue-engineered vascular grafts: overview of recent advancements, *Biomolecules*, 2023, **13**, 1389.
43 J. Xue, T. Wu, Y. Dai and Y. Xia, Electrospinning and electrospun nanofibers: methods, materials, and applications, *Chem. Rev.*, 2019, **119**, 5298–5415.
44 H. F. Motiwala, A. M. Armaly, J. G. Cacioppo, T. C. Coombs, K. R. K. Koehn, V. M. Norwood and J. Aubé, HFIP in organic synthesis, *Chem. Rev.*, 2022, **122**, 12544–12747.
45 O. Hartman, C. Zhang, E. L. Adams, M. C. Farach-Carson, N. J. Petrelli, B. D. Chase and J. F. Rabolt, Biofunctionalization of electrospun PCL-based scaffolds with perlecan domain IV peptide to create a 3-D pharmacokinetic cancer model, *Biomaterials*, 2010, **31**, 5700–5718.
46 D. A. Pompa-Monroy, R. Vera-Graziano, S. G. Dastager, G. L. Pérez-González, N. Bogdanchikova, A. L. Iglesias and L. J. Villarreal-Gómez, Low-cost gelatin/collagen scaffolds for bacterial growth in bioreactors for biotechnology, *Appl. Microbiol. Biotechnol.*, 2025, **109**, 113.
47 E. Majidnia, M. Ahmadian, H. Salehi and N. Amirpour, Development of an electrospun poly(ε-caprolactone)/collagen-based human amniotic membrane powder scaffold for culturing retinal pigment epithelial cells, *Sci. Rep.*, 2022, **12**, 6469.
48 J. M. Deitzel, J. Kleinmeyer, D. Harris and N. C. Beck Tan, The effect of processing variables on the morphology of electrospun nanofibers and textiles, *Polymer*, 2001, **42**, 261–272.
49 M. M. Hohman, M. Shin, G. Rutledge and M. P. Brenner, Electrospinning and electrically forced jets. I. Stability theory, *Phys. Fluids*, 2001, **13**, 2201–2220.
50 S. V. Fridrikh, J. H. Yu, M. P. Brenner and G. C. Rutledge, Controlling the fiber diameter during electrospinning, *Phys. Rev. Lett.*, 2003, **90**, 144502.
51 D. Li and Y. Xia, Electrospinning of nanofibers: reinventing the wheel?, *Adv. Mater.*, 2004, **16**, 1151–1170.
52 E. Luong-Van, L. Grøndahl, K. N. Chua, K. W. Leong, V. Nurcombe and S. M. Cool, Controlled release of heparin from poly(ε-caprolactone) electrospun fibers, *Biomaterials*, 2006, **27**, 2042–2050.
53 X. Kong, Y. He, H. Zhou, P. Gao, L. Xu, Z. Han, L. Yang and M. Wang, Chondroitin sulfate/polycaprolactone/gelatin electrospun nanofibers with antithrombogenicity and enhanced endothelial cell affinity as a potential scaffold for blood vessel tissue engineering, *Nanoscale Res. Lett.*, 2021, **16**, 62.
54 Z. Ebrahimi, S. Irani, A. Ardeshirylajimi and E. Seyedjafari, Enhanced osteogenic differentiation of stem cells by 3D printed PCL scaffolds coated with collagen and hydroxyapatite, *Sci. Rep.*, 2022, **12**, 12359.
55 B. Feng, T. Ji, X. Wang, W. Fu, L. Ye, H. Zhang and F. Li, Engineering cartilage tissue based on cartilage-derived extracellular matrix cECM/PCL hybrid nanofibrous scaffold, *Mater. Des.*, 2020, **193**, 108773.
56 Z. Syedain, J. Reimer, M. Lahti, J. Berry, S. Johnson, R. Bianco and R. T. Tranquillo, Tissue engineering of acellular vascular grafts capable of somatic growth in young lambs, *Nat. Commun.*, 2016, **7**, 12951.
57 J. A. Reid and A. Callanan, Hybrid cardiovascular sourced extracellular matrix scaffolds as possible platforms for vascular tissue engineering, *J. Biomed. Mater. Res., Part B*, 2020, **108**, 910–924.
58 B. Xia, D. H. Kim, S. Bansal, Y. Bae, R. L. Mauck and S. J. Heo, Development of a decellularized meniscus matrix-based nanofibrous scaffold for meniscus tissue engineering, *Acta Biomater.*, 2021, **128**, 175–185.
59 Y. Gao, V. L. Gadd, M. Heim, R. Grant, T. S. R. Bate, H. Esser, S. Ferreira Gonzalez, T. Y. Man, S. J. Forbes and A. Callanan, Combining human liver ECM with topographically featured electrospun scaffolds for engineering hepatic microenvironment, *Sci. Rep.*, 2024, **14**, 23192.
60 D. V. Bax, N. Davidenko, D. Gullberg, S. W. Hamaia, R. W. Farndale, S. M. Best and R. E. Cameron,

Fundamental insight into the effect of carbodiimide crosslinking on cellular recognition of collagen-based scaffolds, *Acta Biomater.*, 2017, **49**, 218–234.

61 M. T. Ngo and B. A. C. Harley, Angiogenic biomaterials to promote therapeutic regeneration and investigate disease progression, *Biomaterials*, 2020, **255**, 120207.

62 Z. Lang, T. Chen, S. Zhu, X. Wu, Y. Wu, X. Miao, Q. Wang, L. Zhao, Z. Zhu and R. X. Xu, Construction of vascular grafts based on tissue-engineered scaffolds, *Mater. Today Bio*, 2024, **29**, 101336.

63 P. K. Thalla, H. Fadlallah, B. Liberelle, P. Lequoy, G. De Crescenzo, Y. Merhi and S. Lerouge, Chondroitin sulfate coatings display low platelet but high endothelial cell adhesive properties favorable for vascular implants, *Biomacromolecules*, 2014, **15**, 2512–2520.

64 Y. Niu and M. Galluzzi, Hyaluronic acid/collagen nanofiber tubular scaffolds support endothelial cell proliferation, phenotypic shape and endothelialization, *Nanomaterials*, 2021, **11**, 2334.